Experimental study of fluctuations excited by a narrow temperature filament in a magnetized plasma

A. T. Burke, J. E. Maggs, and G. J. Morales
Department of Physics and Astronomy, University of California, Los Angeles, California 90095

(Received 15 November 1999; accepted 3 February 2000)

A systematic study is made of the spontaneous growth of fluctuations in temperature, density, and magnetic field in a narrow (on the order of the electron skin depth) field-aligned temperature filament embedded in a large magnetized plasma. Two broad classes of fluctuation (''low'' and ''high'' frequency modes) have been identified and studied in detail. A high-frequency drift-Alfvén mode grows at frequencies about one tenth the ion gyrofrequency in the region of the filament where the temperature gradient is large. The measured radial profiles of the density and magnetic field fluctuations associated with this mode agree well with theoretical predictions. The high-frequency mode has been observed to exhibit several interesting nonlinear features, including steepening wave form, progression in azimuthal mode number, coupling to the low frequency mode with subsequent sideband generation, and eventually a transition to broad band turbulence. The nature of the low-frequency mode which has frequencies about one fiftieth of the ion gyrofrequency is less certain, but it has been identified as a spatially localized, azimuthally symmetric mode consisting primarily of temperature fluctuations. Both the high and low-frequency modes give rise to electron heat transport at rates in excess of the classical values. © *2000 American Institute of Physics.* [S1070-664X(00)02605-7]

I. INTRODUCTION

Electron heat transport in magnetized plasmas is a fundamental topic of interest to several areas of contemporary research in plasma science. It is commonly observed that the rate of heat transport associated with electrons substantially exceeds the prediction of classical transport theory based on Coulomb collisions. This anomaly is widely perceived to be the result of spontaneous fluctuations triggered by gradients in the ambient plasma parameters (e.g., density, temperature, magnetic field). As is well known, in neutral gases a localized increase in temperature gives rise to spectacular three dimensional structures (e.g., thunderstorms, tornadoes, hurricanes) that radically alter the transport of heat and mass. By contrast, in a strongly magnetized plasma the confining pressure provided by the magnetic field can arrest the growth of such structure and thus quiescent regions of elevated temperature can be maintained, which is the central idea behind magnetic fusion research. However, for a given magnetic field strength there is a limit on the magnitude of the temperature gradient beyond which fluctuations induce a transition away from classical transport. The present experimental study aims to document the spatio-temporal properties of the spontaneous fluctuations exhibited by a controlled electron temperature filament that exceeds such a limit.

The concept behind the experimental arrangement consists of the creation of a narrow (on the order of the electron skin-depth) temperature filament embedded within a large, magnetized plasma. Such conditions can be achieved by the injection of a small, low-voltage beam in plasmas produced in the Large Plasma Device (LAPD)[1] at the University of California, Los Angeles. For parameter choices that result in quiescent conditions, it is possible to create expanding heat plumes in which heat is observed[2,3] to be conducted at the classical rates,[4,5] along as well as across the confining magnetic field. By increasing the heating power of the electron beam and/or improving the radial confinement by operating at larger magnetic fields, an environment is obtained in which spontaneous fluctuations develop and significant departures from classical transport are measured. The fluctuations that develop are of two different types. A higher frequency mode consisting of density and magnetic field fluctuations has been quantitatively identified as a drift-Alfvén eigenmode that exhibits a remarkable spiral pattern and other azimuthal structure. A lower-frequency mode, highly localized to the center of the filament, has been found to consist of temperature fluctuations that propagate along the magnetic field at speeds faster than the ion acoustic speed.

The paper is organized as follows. Section II describes the experimental setup and the plasma conditions in which the fluctuation studies are made. The properties of the high-frequency fluctuations are presented in Sec. III and the features of the low-frequency phenomena are outlined in Sec. IV. The transport modifications caused by the fluctuations are found in Sec. V. Conclusions are presented in Sec. VI.

II. EXPERIMENTAL SETUP

The fluctuation studies were conducted in the Large Plasma Device (LAPD)[1] at the University of California, Los Angeles. The experimental arrangement is identical to that used previously[2,3] to observe the heat transport exhibited by an expanding temperature plume. A schematic of the experimental setup is shown in Fig. 1. The plasma is generated by electrons (primaries) emitted from a heated, barium oxide

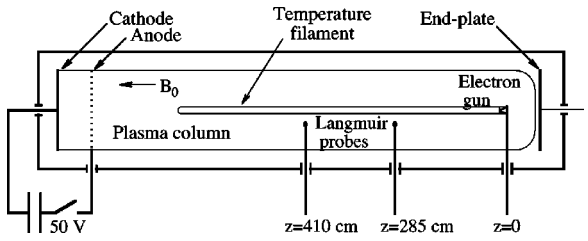

FIG. 1. Schematic of the experimental setup. A small (3 mm) electron beam source is located near the end of the device away from the cathode. A low voltage beam ($\sim$20 V) produces a field-aligned, expanding temperature plume that spontaneously develops fluctuations in temperature, density, and magnetic field. Planes of data are taken at various axial locations along the temperature filament.

coated cathode and subsequently accelerated by a semitransparent (transmission efficiency $\approx$50%) grid anode located 60 cm from the cathode. The end of the plasma column is terminated by an electrically floating copper plate. The accelerated primaries ($\sim$50 V) drift into a 9.4 m long vacuum chamber and strike neutral He gas at a fill pressure of 1.0×10^{-4} torr to generate a 40 cm diameter, He plasma with greater than 75% degree of ionization. Discharge currents of 1–5 kA are used to generate axially and radially uniform plasmas with measured densities $n_e=1.0-4.0\times10^{12}$ cm^{-3}, electron temperatures $T_e=6-8$ eV, and ion temperatures $T_i\simeq1$ eV. Magnetic field strengths in the range of 0.5–1.5 kG are used. The fluctuation studies are performed in the so-called afterglow phase of the plasma, i.e., after the discharge pulse is terminated. In the afterglow plasma T_e decays rapidly (on a time scale of 100 μs) due to classical axial transport to the ends of the device and cooling due to energy transfer to the ions. The plasma density, however, decays slowly (on a time scale of 2 ms) due to ambipolar flow at the sound speed. The experiment consists of injecting a low voltage (15–20 eV) electron beam of small transverse extent (3 mm diameter) into a large plasma generated in the LAPD facility. The beam is produced by biasing a heated, single crystal of lanthanum–hexaboride (LaB_6) with negative polarity relative to the grid anode. The beam-generating crystal is located 75 cm from the end of the plasma column (i.e., 9.25 m from the cathode). Measurements of the electron temperature are taken at four axial locations: 285, 410, 535, and 660 cm from the beam injector.

For the purposes of the present study the ambient plasma is essentially of infinite extent. The fast electrons emitted from the beam cathode are slowed down and thermalized in a fairly short distance due to elastic collisions with the slow bulk plasma electrons and ions (the frictional drag term in the Fokker–Planck equation).[6,7] Under the conditions of the experiments reported here the 20 V beam-electrons are slowed down in a distance of 70 cm. Thus the role of the beam is simply to produce a heat source a few millimeters in diameter and about a meter in length. Typical beam currents of 200 mA are used, resulting in a heat source strength of approximately 0.2 W/cm^3. When these power densities are applied to afterglow plasmas in which the ambient electron temperature decays to a low level of $T_e\lesssim1$ eV at densities $n\sim2\times10^{12}$ cm^{-3}, it is possible to locally increase T_e by 5 $-$10 times the ambient value, thus generating steep temperature gradients which spontaneously develop large fluctuations in density, temperature, and magnetic field.

The fluctuations in density and temperature are deduced from the current–voltage characteristics (I–V) of a small ($\sim$1 mm^2) flattened-tip Langmuir probe. Using I–V traces from Langmuir probes has the advantage that the temperature, density, and plasma potential can be obtained. The principal disadvantage of this technique in the present study is that it takes a finite time interval to obtain the curves due to the requirement of a voltage sweep. Also the great variation in temperature from outside the heated filament where the plasma may be a few tenths of an eV to inside the filament where the temperature is several eV requires different sweep rates for optimal measurement. While a rapid sweep rate of several volts per microsecond can be used in the hot regions, the cold plasma region requires sweep rates of a few tenths of a volt per microsecond. Thus it can take about a hundred microseconds to measure the temperature using voltage sweeps, so that it is not possible to easily discern fluctuations in temperature or density with this technique.

This difficulty can be overcome by using ion saturation current as a measure of the electron temperature. In plasmas with $T_i\lesssim T_e$, the ion saturation current is insensitive to T_i and can be taken as proportional to $n_eT_e^{1/2}$.[8] Thus the electron temperature can be measured using ion saturation current if the plasma density can be determined by other means. Since the beam does not produce ionization,[3] the plasma density in the beam heated region can be taken to be equal to the density in the center of the plasma column. We determine the density of the plasma column by using the phase shift measured by a 56 GHz interferometer[9] located a distance 130 cm from the beam injection point. The interferometer measures a column average plasma density. Langmuir traces are used to obtain a relative density profile of the column which is then used in conjunction with the interferometer data to obtain a calibrated density profile across the column. The interferometer gives a continuous readout of the phase shift so that instantaneous column averaged density measurements are available.

In this study we use the following expression for the electron temperature:

$$T_e(\vec{r},t)=T_e^0\left(\frac{I_{\rm sat}(\vec{r},t)}{I_{\rm sat}^0}\right)^2\left(\frac{n_e^0}{n_e(t)}\right)^2, \tag{1}$$

where the calibration parameters $I_{\rm sat}^0$, T_e^0, and n_e^0 correspond to measurements at a single time and location. Typically, the calibration parameters are measured just before beam injection. The continuous plasma density $n_e(t)$ is obtained from the 56 GHz interferometer. Figure 2 shows a comparison between temperature measurements obtained using swept Langmuir voltage traces and those obtained from Eq. (1) using ion saturation measurements. The two curves agree over most of the temperature range sampled to within experimental error. The temperature measurements used in this study were obtained using the ion saturation current technique described here. To further ascertain that the $I_{\rm sat}$ measurements are not contaminated by beam produced ioniza-

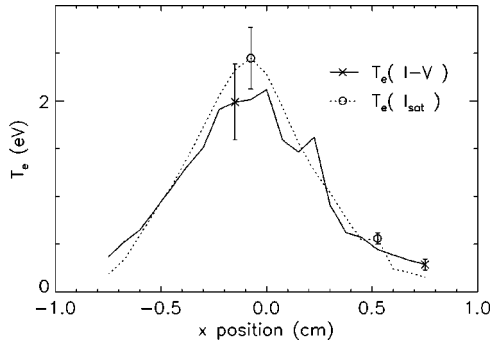

FIG. 2. Comparison of a voltage-swept, Langmuir probe measurement (solid curve) of the filament temperature profile with a calibrated ion saturation current (I_{sat}) measurement (dotted curve). The degree to which these curves agree indicates the accuracy of the I_{sat} measurement method used to deduce the value of the electron temperature.

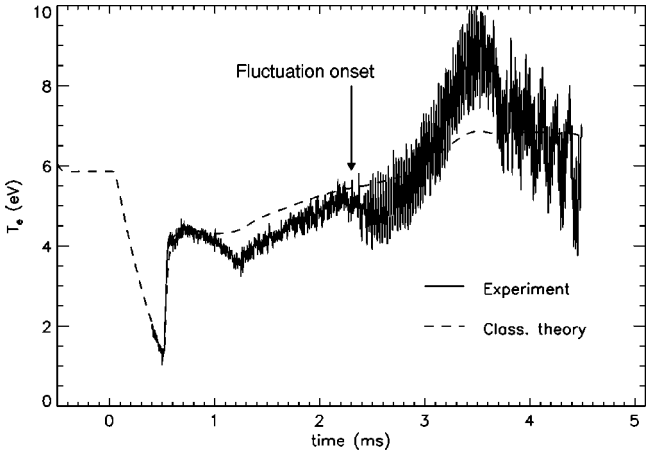

FIG. 3. I_{sat} signal (noisy curve) at the center of the temperature filament converted to electron temperature illustrates that, after an extended period of classical transport, a coherent high-frequency mode develops, followed by the onset of low-frequency fluctuations. Dashed curve is the predicted evolution of the electron temperature according to classical theory. Discharge current is turned off at $t=0$, and heating beam is applied at $t=0.5$ ms. Axial location is 285 cm from the beam injector.

tion, we have examined the temporal decay of the signal after rapid turn off of the beam. It is found that the I_{sat} signal decays on the fast time scale expected of a temperature change.

The magnetic field fluctuations are measured with small (2 mm) dB/dt loops that permit the determination of the local magnetic field vector in the two dimensions perpendicular to the confining magnetic field. The component of the magnetic fluctuations along the magnetic field, for the phenomena investigated here, was measured separately to be within the experimental noise level, i.e., the modes have shear polarization.

III. HIGH-FREQUENCY FLUCTUATIONS

To illuminate the role of spontaneous fluctuations in electron heat transport we first present an example in which a temperature filament that exhibits radial and axial heat transport at the classically predicted rates for a significant time interval (approximately 1000 ion gyroperiods), eventually undergoes a transition to fluctuation-dominated behavior.

Figure 3 displays the time evolution of the electron temperature T_e at the center of the filament ($r=0$) and at an axial distance 285 cm from the beam injector. The dashed curve in Fig. 3 corresponds to the prediction of a two-dimensional, time-dependent, nonlinear transport code based on the classical heat transport coefficients.[3] The continuous noisy trace is the value of T_e deduced from the ion saturation current according to the procedure explained in Sec. II. The beam is injected at $t=0.5$ ms after the termination of the voltage pulse between the anode and cathode, i.e., during the afterglow phase. It is seen that the heat source provided by the beam increases the temperature of the afterglow plasma as predicted by classical theory for an interval of approximately 2 ms. At this time it is observed that high-frequency fluctuations develop in the ion saturation current and, at this axial location, are accompanied by a slight decrease, followed by a sharp increase in the average temperature. At about 3 ms after beam injection low-frequency oscillations appear in I_{sat} and, simultaneously, the average slope of the curve undergoes a sharp drop, thus indicating an enhanced rate of heat transport. Since I_{sat} is the product of n_e and $T_e^{1/2}$, fluctuations in the ion saturation current can be either due to changes in the temperature, density or both. Although we present the I_{sat} signal in Fig. 3 as temperature this designation actually applies only to the average value of the trace. A detailed examination of the fluctuating signals indicates that the high-frequency fluctuations seen in Fig. 3 are associated with density changes while the low-frequency signals are primarily electron temperature fluctuations. We have determined that the high frequency fluctuations in the ion saturation current are primarily due to changes in density by comparing measurements of ion saturation current with density and temperature measurements obtained from I–V curves from a rapidly swept (10 V/μs) Langmuir probe. We found that, for high frequencies, the fluctuations in density as determined from the Langmuir traces correlated with fluctuations in the ion saturation current with a correlation coefficient of 0.86. On the other hand, fluctuations in $T_e^{1/2}$ correlated with the ion saturation current with a coefficient of only 0.5. Moreover, the normalized fluctuation amplitudes of I_{sat} and $\tilde{n}_e$ agree within 10 percent while the normalized fluctuation amplitude of $T_e^{1/2}$ is about half that of I_{sat}. The method used to determine that the low-frequency fluctuations are temperature changes is discussed later.

Next we present results in which the various parameters are chosen so that the fluctuations develop much earlier than in the case presented in Fig. 3, i.e., the interval during which classical transport occurs is significantly reduced. Nearly instantaneous onset of high-frequency fluctuations can be realized by moving the onset of the beam pulse further into the afterglow plasma when the electron temperature and density of the bulk plasma are lower. Using a specifically built probe that incorporates an operating Langmuir probe and two dB/dt loops it is possible to simultaneously map the two-dimensional structure (across the confining magnetic field) of the self-consistent fluctuations in ion saturation current and magnetic field associated with the high-frequency fluctua-

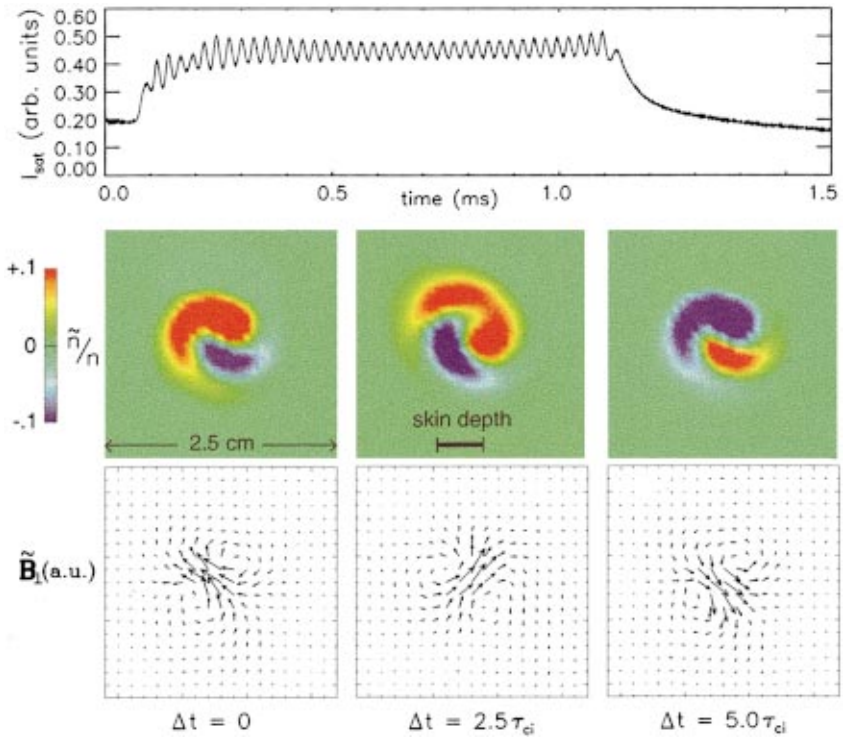

FIG. 4. (Color) Middle: Time evolution of structure across the confining magnetic field of high-frequency density fluctuations. Red color denotes a density increase, and blue a decrease, relative to the average value. Bottom: Self-consistent magnetic fluctuations having shear-mode polarization. Rotation is in the direction of the electron diamagnetic drift. Top: Temporal variation of the ion saturation current at a radial location near the steepest gradient in the temperature profile. The ion cyclotron period is τ_{ci}.

tions. Figure 4 shows the spatial and temporal dependence of the spontaneous fluctuations occurring in a filament produced by a beam pulse of 1.1 ms duration injected at $t=3.0$ ms into the afterglow plasma. The data plane is at an axial location 410 cm from the beam injector. The top panel of Fig. 4 shows the temporal variation of the ion saturation current at a radial location near the steepest gradient in the temperature profile ($r=3$ mm). The middle panel displays the oscillations in density, $\tilde{n}$, at three selected times over an interval of five ion gyroperiods or about one-half of the fluctuation period. The red color represents an increase, and blue a decrease, relative to the average value. This figure is obtained by taking an average over 20, highly reproducible plasma pulses (at a repetition rate of 1 Hz) at every spatial location (with a grid resolution of 1.5 mm interpolated to 0.75 mm), thus indicating that the spontaneously generated structure undergoes phase locking and that the fluctuations remain coherent over a significant time interval (greater than 100 ion gyroperiods). It is evident from Fig. 4 that the $\tilde{n}$ signal has an azimuthal mode number $m=1$ and displays a spiral structure that can give rise to radial transport. Simultaneously with the fluctuations in density there appear fluctuations in the magnetic field $\tilde{B}$ in the direction transverse to the confining field (i.e., shear polarization), as shown in the bottom panel of Fig. 4. It is found that the magnetic structure is like a rotating dipole with a peak field at the center of the filament; physically it is generated by two microscopic axial currents, embedded within the temperature filament (whose transverse scale is on the order of the electron skin depth, as indicated in Fig. 2), which rotate around the center of the filament. The sense of rotation of $\tilde{n}$ and $\tilde{B}$ corresponds to the direction of the electron diamagnetic drift associated with the transverse gradient in T_e. It should be emphasized that, over the entire time record shown in the top panel of Fig. 4, the azimuthal structure of the density fluctuation remains an $m=1$ mode. (This behavior is in contrast to the mode-progression phenomena illustrated later in Fig. 11.)

Since the dual probe (with the dB/dt loops) used to measure the simultaneous fluctuations in density and magnetic field is larger than a single Langmuir probe, some of the detailed variations in the spiral structure shown in Fig. 4 (such as the difference in the shape of the two spiral arms) is due to probe shadowing. Shadowing occurs when this larger probe and probe shaft intersect the temperature filament. These effects can be clearly identified as probe shadowing both because of where they occur, and the fact they are not present when a single small Langmuir probe is used. For completeness, it should be mentioned that this is not the first experiment in which a spiral structure has been observed in a plasma. A phase-locked spiral ($m=2$) has been previously observed[10] in an argon plasma column generated by electron cyclotron waves, and a persistent spiral-arm structure has been formed in a rotating plasma embedded in a stationary gas.[11]

Figure 5 shows the frequency spectrum (in log scale) of the ion saturation current (solid curve) and the magnetic fluctuations (dotted curve) measured at $r=0.1$ cm at an axial position 285 cm away from the beam injector for the case shown in Fig. 3 for a 1 ms long time-window centered around $t=4$ ms. This case is illustrative of frequency spectra just after the onset of low-frequency fluctuations. The ion saturation current and magnetic spectra are very similar. The high-frequency mode at 50 kHz, whose spatial configuration is like the spiral structure shown in Fig. 4, shows sidebands at about 40 and 60 kHz around the central frequency. These sidebands are indicative of an interaction between the high- and low-frequency modes. The second harmonic signal generated by this structure (centered around 95 kHz) also exhib-

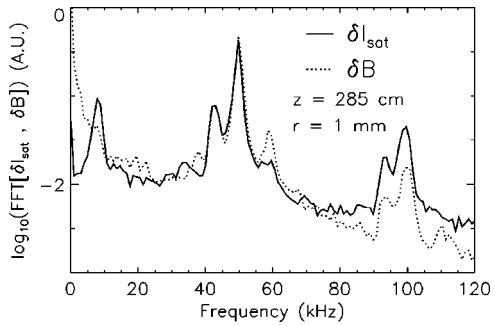

FIG. 5. Frequency spectrum (log scale) of fluctuations in the ion saturation current and magnetic field near the center of the temperature filament at an axial location 285 cm from the beam injector. Ion cyclotron frequency is 380 kHz.

its sidebands in the density and magnetic field fluctuations. In contrast, the low-frequency mode identified in Fig. 4, does not have an identifiable peak (i.e., one clearly above the noise level) in the magnetic signal.

Due to the elongated nature of the temperature filament and the very narrow transverse extent (a few mm) it is quite difficult to perform meaningful measurements of the axial wavelength associated with the fluctuations. A complementary measurement that gives an indication of the axial nature of the high-frequency signal is shown in Fig. 6. The frequency spectrum (log scale) of the ion saturation current measured at a radial location $r=4$ mm from the center of the filament is shown for two axial positions separated by 125 cm. The high-frequency peak at 40 kHz, associated with a spiral structure of the type shown in Fig. 4, indeed extends over this interval. This observation is consistent with the interpretation that this structure is a global eigenmode of the temperature filament. The experimental conditions under which Fig. 6 was obtained differ from those leading to Fig. 5. Consequently, no inference should be drawn from the observed fact that the frequencies of the eigenmodes displayed in these two figures are different.

To quantitatively identify the nature of the high-frequency fluctuations we compare the measured radial structure of the density and magnetic fluctuations with a theoretical calculation of unstable drift-Alfvén eigenmodes.[12] The theory describes the electron behavior kinetically and includes the important effect of velocity-dependent pitch-

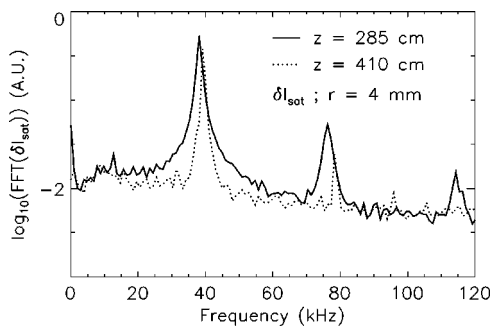

FIG. 6. Comparison of frequency spectrum (log scale) of ion saturation current at two axial positions, separated by 125 cm, indicates that the high-frequency fluctuation is a global mode.

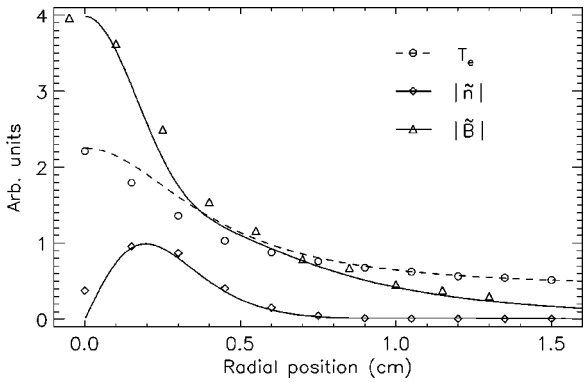

FIG. 7. Comparison between experimental measurements (discrete points) and theoretical predictions (solid curves) for the radial structure of the density and magnetic fluctuations associated with the most unstable drift-Alfvén eigenmode. The dashed curve, an analytic fit to the measured temperature profile, is used in the theoretical analysis.

angle scattering (Lorentz model). The ion response is taken to be that of a cold, magnetized fluid (in the experiment $T_i \sim 0.5-1$ eV). The open symbols in Fig. 7 are the experimental measurements while the solid lines correspond to the theoretically predicted fastest growing mode ($m=1$). The dashed line is an analytical fit to the measured temperature profile. The analytical fit is used to facilitate the eigenmode calculation. It is found that the predicted radial structure of the most unstable drift-Alfvén mode is in excellent agreement with the observations. However, the predicted frequency is 26 kHz while the experimentally observed value is 38 kHz. This discrepancy suggests the possibility that a Doppler-shift due to a static electric field in the radial direction may be contributing to the observed value in the stationary probe frame. However, due to the small value of the radius where the frequency is measured (a few mm), the associated azimuthal wave number ($\simeq 1/r$) is large, and the radial electric field associated with a 10 kHz Doppler shift is $\leqslant 0.2$ V/cm. Such a small electric field is not measurable with the techniques currently available. Of course, there may be additional effects not included in the theory which may not alter the radial structure, but give a small change in the real part of the eigenvalue. It should be mentioned that using the complex eigenfunctions of the theory it is possible to generate time dependent displays that also exhibit the experimentally observed spiral structure shown in Fig. 4. However, for brevity, these results are not presented here. It is noteworthy that the observed growth rate of the drift-Alfvén eigenmode is comparable to its frequency, as predicted theoretically (e.g., Fig. 12 in Ref. 12). For this reason it is difficult, experimentally, to obtain a satisfactory measurement of its value.

A brief cautionary note is warranted in the comparison of the measurements to linear theory. Since the modes exhibit a large growth rate, the eigenfunctions shown in Fig. 7 have been measured in the nonlinear, saturated state. However, as is frequently the case in problems of this type, even under strongly nonlinear conditions the linear eigenmodes are not significantly distorted.

The dependence of the frequency of oscillation on the

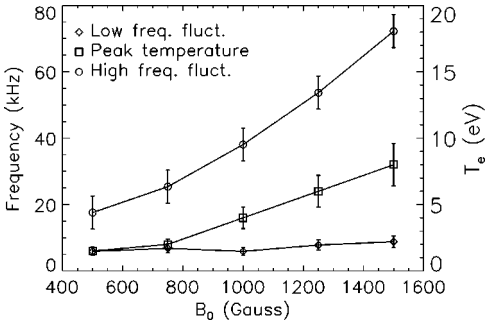

FIG. 8. Dependence of the frequencies of the high- and low-frequency modes on the strength of the confining magnetic field. Increase in peak temperature of the filament (right-hand scale) is the result of improved radial confinement as magnetic field strength increases.

strength of the confining magnetic field is shown in Fig. 8 for the high- and low-frequency modes illustrated by Fig. 3. The associated dependence of the peak electron temperature (i.e., at $r=0$) is also shown and, as expected, it is seen to increase as the radial heat confinement is improved. It is seen that the measured frequency of the mode identified as a drift-Alfvén eigenmode shows a nearly linear increase with field strength, consistent with the increase in Alfvén speed. In contrast, the low-frequency mode is insensitive to changes in magnetic field and/or electron temperature.

Having identified the high-frequency mode as a drift-Alfvén wave, we next proceed to outline some of the nonlinear features that occur as its amplitude grows to significant levels. To appreciate the richness and complexity of the nonlinear processes, it must be emphasized that these modes have a three-dimensional structure whose properties are determined by nonlocal effects associated with the radial gradient, axial extent, and temperature of the filament. The spatio-temporal behavior of the filament is, of course, determined by nonlinearities intrinsic to the classical transport coefficients together with the enhanced transport caused by the mode whose nonlinear features one would like to identify.

A common nonlinearity expected to arise from a coherent eigenmode is the self-distortion of the waveform due to harmonic generation. Indeed such a phenomenon is clearly observed in situations in which the growth of the high-frequency mode is well separated temporally from the appearance of the low-frequency mode, as is the case illustrated in Fig. 3 over the time interval from 2 to 3 ms. Strong harmonic distortions appear at radial locations in the neighborhood of the peak of the eigenfunction (shown in Fig. 7). An example of the development of such a process is illustrated in Fig. 9 which shows the spectrum (log scale) of the ion saturation current measured at a radial position $r=3$ mm from the center of the filament and an axial location 285 cm from the beam injector. The three different panels shown in Fig. 9 correspond to the behavior at different time intervals after the heat source is turned on ($t=0$). The top panel corresponds to the early stage in which a lower amplitude signal exhibits a single frequency peak (the eigenfrequency of the mode). A sample of the associated sinusoidal waveform is shown at the top right-hand side of the panel. The center

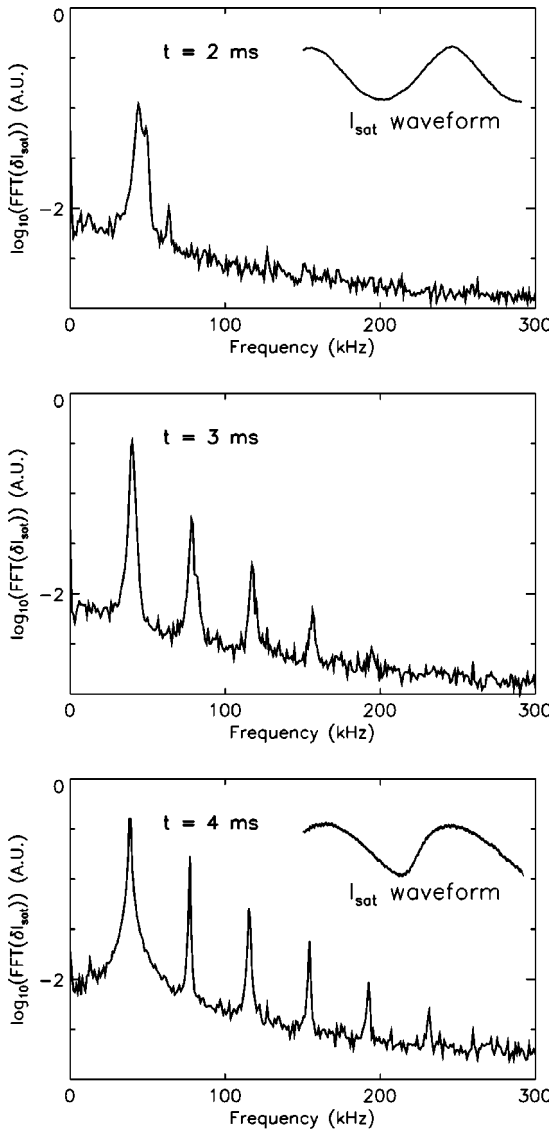

FIG. 9. Frequency spectrum (log scale) of ion saturation current at different times in the evolution of the coherent spiral structure shows development of harmonic distortion associated with steepening of waveform as amplitude increases.

panel indicates an intermediate stage in which a larger amplitude is achieved. Three harmonic peaks in addition to the fundamental are clearly present. The bottom panel shows the late behavior in which the waveform of the drift-Alfvén eigenmode is strongly steepened as indicated by the sample waveform at the upper right of the panel. At this late time, over five additional harmonic peaks are discernable in the spectrum.

Another type of nonlinear modification is associated with the adiabatic change of the eigenmode frequency as the filament parameters vary in time (e.g., a change in the axial length of the filament). Such a phenomenon is illustrated in Fig. 10 for various spiral structures generated at different values of the confining magnetic field in the range 0.5–1.5 kG. The eigenfrequency of the spiral exhibits a small, but systematic, decrease as the filament evolves in time. This behavior holds over the wide range of temperature filaments sampled. The variation in filament properties is considerable

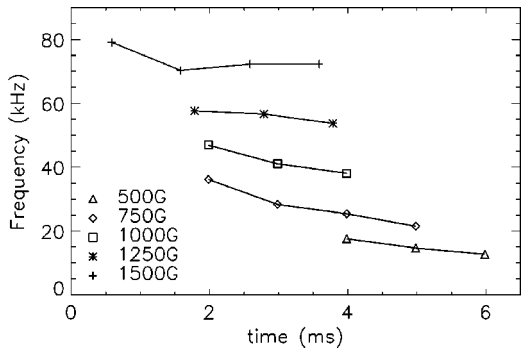

FIG. 10. Slow-time variation of the frequency of the coherent spiral structure at various magnetic field strengths.

because the classical heat transport coefficient, $\kappa_\perp$ with its B^{-2} behavior changes by a factor of 10 over the range of magnetic field strength shown. In addition, close inspection of Fig. 9 indicates that while the process of harmonic generation occurs the frequency of the fundamental mode also decreases in time. For completeness, we note that presently there is considerable interest in nonlinear dynamics studies of saturated instabilities that exhibit frequency sweeping phenomena.

As shown in Fig. 11, the spiral structure can also exhibit a very striking topological change corresponding to a steady progression of the azimuthal mode number, *m*. From an initial $m=1$ eigenmode, the mode progresses to the nearest *m*-mode number eventually reaching mode numbers in excess of $m=6$. The progression occurs without a discernable feature in the time signature sampled at a given radial position, i.e., the frequencies of neighboring modes with different *m* number are nearly degenerate. Such near degeneracy is indeed predicted by the same theoretical analysis[12] that explains the radial structure of the measured eigenmodes previously illustrated in Fig. 7. The three color panels at the top of Fig. 11 depict the two-dimensional pattern of the ion saturation current fluctuations for three different time intervals. The method of presentation is the same as in Fig. 4, but now the time interval over which the spiral structure is sampled exceeds 380 ion gyroperiods (i.e., over 70-times longer than in Fig. 4). The temporal behavior of the ion saturation current measured at a fixed spatial position across the magnetic field ($x=4$ mm, $y=7.5$ mm; indicated by the **x** symbol in the first color panel) is shown in the bottom panel of Fig. 11. The arrows indicate the time on the ion saturation trace corresponding to each color panel. In the data plane across the magnetic field, the temperature contours of the filament are observed to become azimuthally asymmetric, while mode progression is occurring. The process of mode progression must arise from the azimuthal distortion in the temperature filament. This behavior is in contrast to the situation described in Fig. 4 in which no mode progression develops over an equivalent time period. In the case shown in Fig. 4, however, the temperature profile remains azimuthally symmetric.

It should be noted that the oscillation frequency of the measured signal does not change as the *m* number increases. In fact, examination of the peak-to-peak period of the signal shows that the period is constant within experimental uncertainty. Because the frequency of the oscillations observed at a fixed spatial location remains constant as the *m* number increases (i.e., the azimuthal wavelength decreases) the rate of rotation of the structure must decrease, as indeed is observed. It is also measured that, as the *m* number increases, the eigenfunction becomes flatter near the center of the temperature profile, as expected of a proper eigenmode.

Although the interval over which high-frequency coherent structures exist and develop interesting coherent nonlinearities is quite large, the long-time behavior of the temperature filament results in signals with a broad frequency spectrum, as illustrated in Fig. 12. The top panel corresponds to the spectrum (log scale) of ion saturation current measured in the center of the filament at an axial location 535 cm from the beam injector 8 ms after beam injection. The bottom panel shows the corresponding spectrum (log scale) of the associated magnetic fluctuations. For reference, in both panels the spectrum in the absence of the temperature filament is

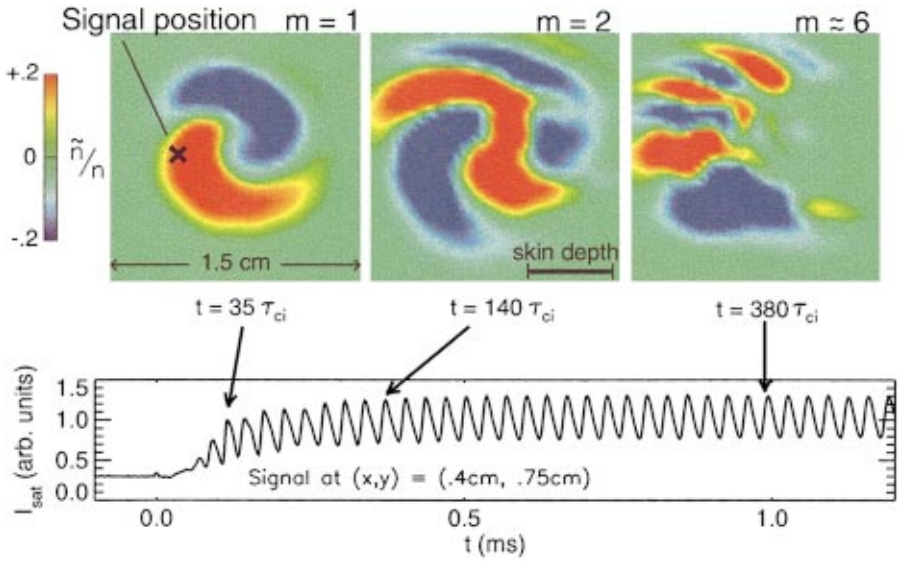

FIG. 11. (Color) Time evolution of the two-dimensional structure across the confining magnetic field of high-frequency mode exhibits a progressive, sequential transition to higher azimuthal mode numbers. Top panel is a display similar to that used in Fig. 4. Bottom panel shows time evolution of ion saturation current at spatial location marked by an *x* in leftmost color panel. The arrows indicate the time when the structure was measured. The ion gyroperiod is τ_{ci}.

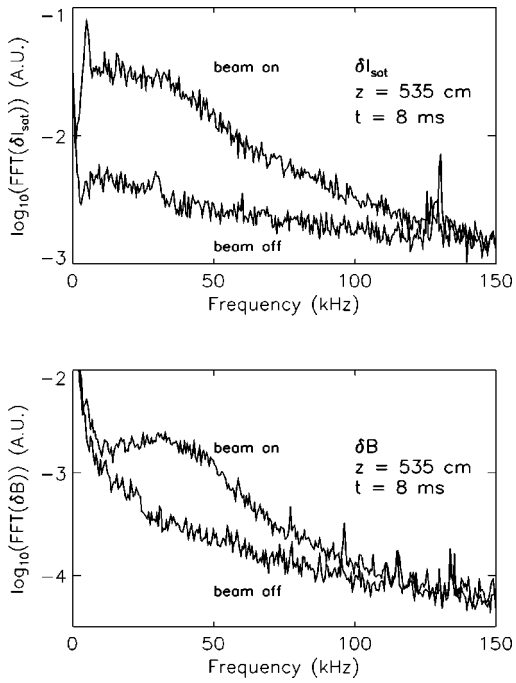

FIG. 12. Typical broadband frequency spectrum (log scale) exhibited by fluctuations in ion saturation current (top panel) and magnetic field (bottom panel) at late times and large axial positions at higher magnetic field strength (1.5 kG). Bottom curves in both panels correspond to ambient spectra in the absence of temperature filament.

also shown. The only evidence for a coherent signal is the low-frequency peak seen in the ion saturation current. The magnetic spectrum in Fig. 12 exhibits a broad peak centered around the frequency of the $m=1$ mode identified at earlier times to be a coherent spiral.

IV. LOW-FREQUENCY FLUCTUATIONS

We do not, presently, have a theoretical understanding of the nature of the low-frequency phenomena. This section presents results of experimental studies of the principal features of the low-frequency fluctuations in order to help guide future theoretical investigations. An example which illuminates the temporal and spatial evolution of the low-frequency fluctuations is given in Fig. 13 which shows the temporal

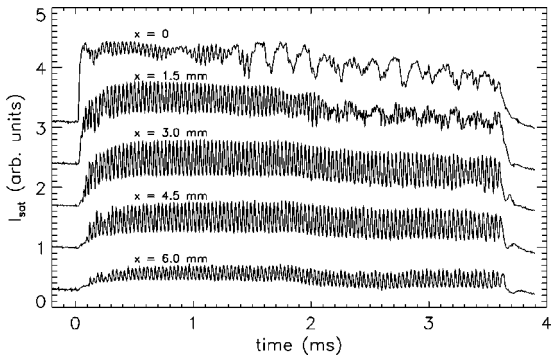

FIG. 13. Time evolution of ion saturation current at four different radial positions across the temperature filament, showing the onset and development of low-frequency oscillations near the center ($x=0$, the origin is not the same as in Fig. 14). Axial distance from beam injector is 285 cm.

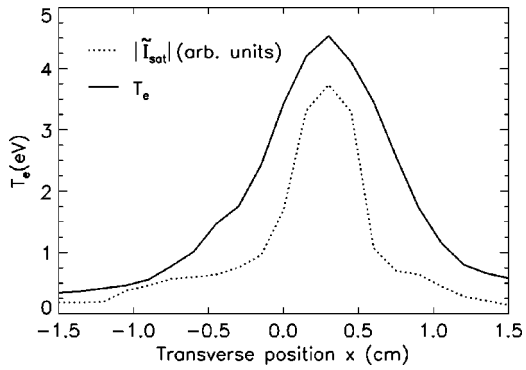

FIG. 14. Dependence of the amplitude of the low-frequency mode on distance across the confining magnetic field (dotted curve). Solid curve corresponds to the temperature profile of the filament at time $t=3$ ms in Fig. 13.

evolution of I_{sat} at various radial positions across a temperature filament at an axial distance 285 cm away from the beam injector. For this case a pulsed beam is initiated late into the afterglow plasma (2.5 ms after shutoff of the discharge pulse). High-frequency fluctuations (frequency ~ 31 kHz) appear almost immediately followed, at the center of the filament, by the onset of low-frequency fluctuations (frequency ~ 8 kHz) of considerable amplitude. The low-frequency fluctuations are initially localized to the center of the filament but broaden as time progresses.

The radial localization of the low-frequency mode is quantified by acquiring ion saturation current and swept voltage, Langmuir I–V traces on a spatial grid with spacing of 0.75 mm. Figure 14 displays the radial dependence of the electron temperature (solid curve) along a radial cut across the temperature filament, and the amplitude of the low-frequency fluctuations (dotted curve). In contrast to the high-frequency density eigenfunction, shown in Fig. 7, the low-frequency structure peaks at the center of the filament and thus must be identified as a $m=0$ mode. This feature implies that the mode is not directly driven by diamagnetic currents and consequently not sensitive to the radial temperature gradient. Both of these features are in turn consistent with the insensitivity of the low-frequency mode to changes in magnetic field and/or peak temperature displayed earlier in Fig. 8.

It is very natural to propose that the low-frequency mode is some form of an unstable ion acoustic wave. To check on such a possibility we have performed two separate tests. One consists of a determination of the temporal cross-correlation function of the ion saturation current measured by two probes separated by a distance of 155 cm along the temperature filament, with the closest one being 255 cm from the beam injector. The result is shown in Fig. 15. The display over the large time scale indicates the existence of a highly coherent signal whose frequency is consistent with the frequency determined from the spectral peaks measured at a single axial position by one probe. The inset on Fig. 15 provides a blow-up of the peak of the correlation function over a short time scale. The temporal location in the peak of the cross-correlation function implies the low-frequency signal moves from the location of the upstream probe to the down-

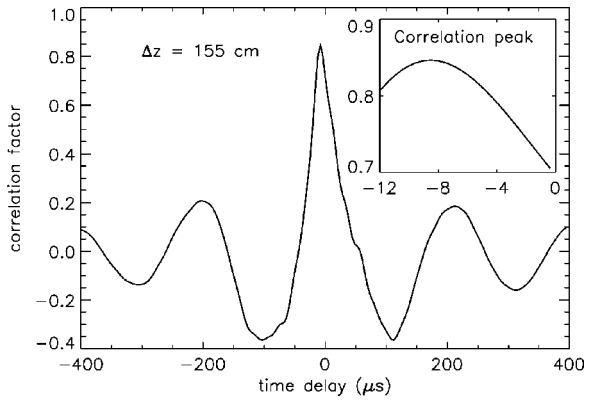

FIG. 15. Cross-correlation function of low-frequency fluctuations in ion saturation current measured by two Langmuir probes within the temperature filament at two different axial locations separated by 155 cm. Details of the correlation peak are shown in the inset.

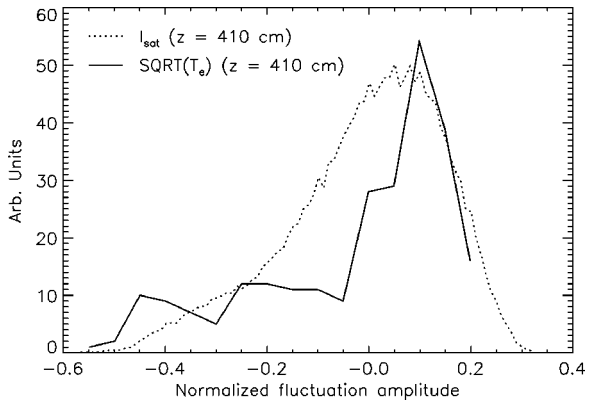

FIG. 16. Comparison between the amplitude distribution function of low-frequency fluctuations in the ion saturation current (dotted curve) and the square-root of electron temperature (solid curve) at an axial location $z = 410$ cm from the beam injector. Negative amplitude means the fluctuation was below the average value, while positive means it was above. Fluctuations are normalized to the average value.

stream probe with a delay time of order 10 μs. Thus the low-frequency mode propagates along the magnetic field in the direction away from the beam injector, i.e., collinear with the injected beam. From the magnitude of the shift of the correlation peak and the separation distance between the probes the axial speed of propagation of the low-frequency mode is computed to be $\sim 2\times 10^7$ cm/s. This propagation speed should be compared with the value of the sound speed $c_s \sim 10^6$ cm/s, the Alfvén speed $v_A \sim 10^8$ cm/s, and the electron thermal speed $\overline{v_e} \sim 10^8$ cm/s at the center of the filament. It can be concluded that the axial propagation speed of the low-frequency mode does not correspond to an ion-acoustic wave nor an Alfvén wave. Since quasi-neutral rearrangements in plasma density are governed by ion acoustic waves this raises the question of what quantity undergoes low-frequency oscillation.

Since the time of axial propagation for the low-frequency mode is on the order of the time scale for axial heat conduction, it is natural to suspect that the low-frequency fluctuations showing up as oscillations in the ion saturation current are due to temperature changes. To determine the nature of the low-frequency fluctuations, we measured, in the middle of a fluctuating filament, the temperature and density by using a rapidly swept (10 V/μs) Langmuir probe. We obtained an ensemble of 256 individual Langmuir I–V traces from separate plasma pulses. In addition we obtained a similar ensemble of ion saturation current fluctuations. Figure 16 shows the distribution of the ensemble of fluctuations in $T_e^{1/2}$ obtained from analysis of the Langmuir I–V traces compared to the distribution of fluctuations in the ion saturation current at axial location $z = 410$ cm. The similarity in the distribution of fluctuations in $I_{\rm sat}$ and $T_e^{1/2}$ leads to the conclusion that the low-frequency fluctuations are due to changes in the electron temperature.

Finally, we discuss some features pertaining to the interaction of the low-frequency mode with the high-frequency mode. We mentioned in discussing Fig. 13 that the low-frequency mode undergoes a radial broadening as time increases. It also appears that at those radial positions where a substantial low-frequency signal is present a quenching of the high-frequency mode develops. It is not conclusive, however, that the quenching is the result of a local process. In fact, it might be simply a self-consistent feature associated with the spiral mode progressing toward higher m numbers which naturally implies a decrease in its amplitude near the center of the filament. An additional aspect of the interaction is illustrated in the top panel of Fig. 12, where it is seen that a clear, coherent peak associated with the low-frequency mode coexists with the broadband drift-Alfvén waves. The significance of this feature is that it corresponds to very late times and large axial locations. Thus, the low-frequency mode retains its long-range coherency at a stage when the heat transport has been significantly modified from the classical behavior.

We close this section by mentioning that we have performed exploratory numerical studies, based on the transport code used to verify the classical transport theory, that shed some light on the possible origin of the low-frequency modes. By postulating that the heat source region (where the initial beam undergoes thermalization) develops a sinusoidal oscillation it is possible to obtain propagating temperature fluctuations at speeds consistent with those deduced from the axial correlation measurement. Also, the radial profile of the oscillatory heat pulses generated is consistent with the measured radial localization. Due to the incomplete and heuristic nature of such a cursory study we do not conclude that this is the definitive explanation, but it should be considered in future studies.

V. ENHANCED TRANSPORT

In the absence of fluctuations it is found that the spatio-temporal evolution of the heat plume generated by the injection of the low-voltage beam expands along the radial and axial directions as predicted by the classical theory of transport based on Coulomb collisions.[3] Classical transport is observed to hold even in situations in which the self-consistent

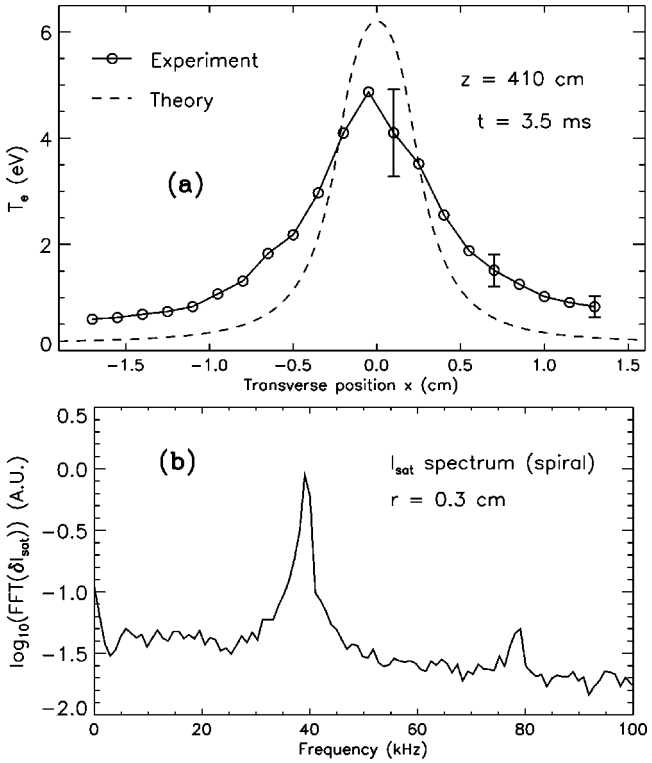

FIG. 17. An example of the departure of heat transport from classical rates in the presence of coherent fluctuations. (a) Measured temperature profile (solid curve) and prediction of classical theory (dashed curve) at an axial location $z=410$ cm from beam injector at a time 3 ms after beam turn on; (b) frequency spectrum (log scale) at a radial position 0.3 cm from the center of the filament.

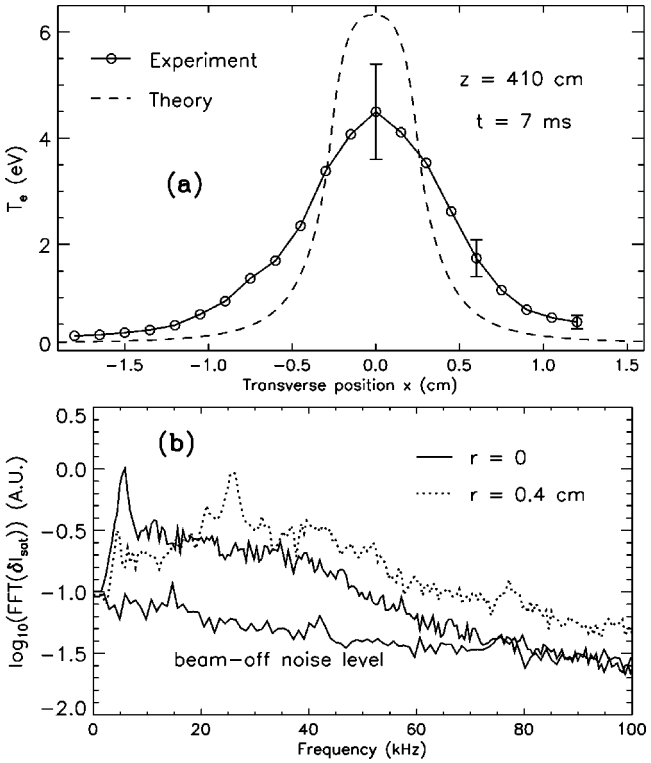

FIG. 18. An example of the departure of transport from classical rates in the presence of broadband fluctuations. (a) Measured temperature profile (solid curve) and prediction of classical theory (dashed curve) at an axial location $z=410$ cm from beam injector at a time 7 ms after beam turn on; (b) frequency spectrum (log scale) of fluctuations in ion saturation current at two different radial positions. Ambient noise level is also shown.

nonlinear variation of the transverse and axial heat conduction coefficients is quite significant (e.g., increases in T_e by a factor of 5 or larger).

When fluctuations develop it is found that the temporal dependence, as well as the radial and axial profiles of the electron temperature, deviates significantly from the classical prediction. As expected, the enhanced transport is a difficult problem to investigate, experimentally and theoretically, because the phenomena is intrinsically three-dimensional, nonlinear and nonlocal. Thus, it is not possible to characterize the behavior with a simple, locally enhanced transport coefficient.

Also, it is difficult to identify a unique property of the fluctuations that causes the enhanced transport. For instance, it is possible to observe enhanced transport under the most coherent situations in which the spectrum of the ion saturation current is dominated by the contribution of the spiral structure associated with a drift-Alfvén eigenmode, and in the absence of low-frequency fluctuations, as is shown in Fig. 17. The bottom panel displays the frequency spectrum (log scale) of the ion saturation current obtained 3.5 ms after beam injection at a radial position $r=0.3$ cm and an axial location $z=410$ cm, for a confining magnetic field of 1.0 kG. The top panel displays both the predicted and measured profiles of the electron temperature across the confining magnetic field. The solid curve is the measured profile and the dashed curve is the profile predicted by classical transport theory. The measured profile is significantly broader than predicted by the classical transport code. The central temperature is lower and, outside the central region, the measured temperature is elevated well above predicted values.

Enhanced transport is also evident when the fluctuations exhibit a more turbulent, broadband character, as illustrated in Fig. 18. In this case the lower panel displays the frequency spectrum (log scale) of the ion saturation current measured at two different radial positions, $r=0$ (solid curve) and $r=0.4$ cm (dotted curve), at an axial location $z=410$ cm from the beam injector. For reference, the frequency spectrum measured in the absence of beam injection is also shown. The top panel of Fig. 18 displays the comparison between the measured and predicted electron temperature profiles at $t=7$ ms after beam injection. It is seen that broadband conditions also give rise to enhanced transport.

VI. CONCLUSIONS

A narrow temperature filament with radial scale size on the order of the electron skin depth, is observed to transition from a state in which heat is conducted throughout the filament by processes governed by Coulomb collisions (classical heat transport) to one in which transport occurs at faster than classical rates. This transition appears to be caused by the onset of fluctuations in plasma density, temperature, and magnetic field. The observed fluctuations fall into two categories: a relatively high-frequency ($f\sim 0.1 f_{ci}$) drift-Alfvén

mode and low-frequency ($f \sim 0.02 f_{ci}$) temperature fluctuations, where f_{ci} is the ion cyclotron frequency.

The high-frequency drift-Alfvén wave is generally the first mode to appear. It is an azimuthally asymmetric mode, generally occurring with a spatial spiral structure that correspond to an $m=1$ azimuthal mode number. Measured density and magnetic field radial profiles for this mode agree well with the predictions of a full electromagnetic theory that includes the effects of Coulomb collisions.[12] This mode has been observed to progress sequentially to higher mode numbers as time advances, reaching mode numbers in excess of $m=6$. In addition the mode undergoes steepening, generating frequency spectra with as many as five observable harmonics in addition to the fundamental frequency.

The low-frequency mode is spatially localized to the central region of the filament and is azimuthally symmetric corresponding to an $m=0$ azimuthal mode number. The low-frequency mode generally occurs after onset of the drift-Alfvén fluctuations and corresponds to fluctuations in the electron temperature. The low-frequency mode couples to the high-frequency mode, generating sidebands and eventually a transition to broadband turbulence.

Both modes are associated with departures from heat conduction at the classical rates.

ACKNOWLEDGMENTS

Research performed by A. T. Burke and G. J. Morales is sponsored by Department of Energy and Office of Naval Research and that of J. E. Maggs by Office of Naval Research and National Science Foundation.

[1] W. Gekelman, H. Pfister, Z. Lucky, J. Bamber, D. Leneman, and J. Maggs, Rev. Sci. Instrum. **62**, 2875 (1991).
[2] A. T. Burke, J. E. Maggs, and G. J. Morales, Phys. Rev. Lett. **81**, 3659 (1998).
[3] A. T. Burke, J. E. Maggs, and G. J. Morales, Phys. Plasmas **7**, 544 (2000).
[4] L. Spitzer, Jr. and R. Härm, Phys. Rev. **89**, 977 (1953).
[5] S. I. Braginskii, *Reviews of Plasma Physics* (Consultants Bureau, New York, 1965), Vol. 1, p. 205.
[6] G. Schmidt, *Physics of High Temperature Plasmas*, 2nd ed. (Academic, New York, 1979), pp. 375–387.
[7] D. L. Book, *NRL Plasma Formulary* (NRL Publication 177-4405, Washington, DC, 1990), pp. 31–33.
[8] F. F. Chen, *Plasma Diagnostic Techniques*, edited by R. H. Huddlestone and S. L. Leonard (Academic, New York, 1965), Sec. 3.3, pp. 138–150.
[9] H. Hutchinson, *Principles of Plasma Diagnostics* (Cambridge University Press, New York, 1987), pp. 95–115.
[10] M. Y. Tanaka, T. Sakamoto, H. Imaizumi, K. Tanaguchi, and Y. Kawai, in *Proceedings of the 1996 International Conference on Plasma Physics, Nagoya, Japan*, edited by H. Sugai and T. Hayashi (International Atomic Energy Agency, Vienna, 1997), Vol. 2, p. 1650.
[11] T. Ikehata, H. Tanaka, N. Y. Sata, and H. Mase, Phys. Rev. Lett. **81**, 1853 (1998).
[12] J. R. Peñano, G. J. Morales, and J. E. Maggs, Phys. Plasmas **7**, 144 (2000).